How to cite: *Angew. Chem. Int. Ed.* **2024**, *63*, e202310112
doi.org/10.1002/anie.202310112

C-H Functionalization

Combinatorial Ligand Assisted Simultaneous Control of Axial and Central Chirality in Highly Stereoselective C–H Allylation

Trisha Bhattacharya, Supratim Ghosh, Subhabrata Dutta, Srimanta Guin, Animesh Ghosh, Haibo Ge, Raghavan B Sunoj,* and Debabrata Maiti**

Abstract: The significance of stereoselective C–H bond functionalization thrives on its direct application potential to pharmaceuticals or complex chiral molecule synthesis. Complication arises when there are multiple stereogenic elements such as a center and an axis of chirality to control. Over the years cooperative assistance of multiple chiral ligands has been applied to control only chiral centers. In this work, we harness the essence of cooperative ligand approach to control two different stereogenic elements in the same molecule by atroposelective allylation to synthesize axially chiral biaryls from its racemic precursor. The crucial roles played by chiral phosphoric acid and chiral amino acid ligand in concert helped us to obtain one major stereoisomer out of four distinct possibilities.

Introduction

The genre of C–H activation has redefined the retrosynthetic disconnection approach for the generation of molecular complexity. It has enabled simple logic that may be applied for rapid access to bio-relevant molecules.[1] However, biologically important molecules usually possess multiple stereocenters in them; hence the use of a stereoselective C–H activation strategy would help broaden its applicability.[2] Notable efforts have been made toward chiral ligand assisted asymmetric C–H bond activation to create central chirality in aliphatic molecules.[2b,3] While for the biaryls, one of the possible modes of inducing asymmetry is by restricting the bond rotation around the biaryl axis which subsequently leads to the development of axial chirality.[4] The atropisomerism due to axial chirality is a general phenomenon observed in *o*,*o*′-substituted biaryls prevalent in various natural products, chiral ligands, catalysts and reagents.[4b,5] However, a C–H activation strategy to induce stereoselective formation of a particular atropisomer remains difficult given the elevated temperature typically used in C–H bond activation reactions that may cause racemization. Nevertheless, the C–H functionalization that restricts the biaryl bond rotation by incorporating hindered functional groups was able to provide atroposelectivity.[6] In one such approach, a chiral sulfone directing group (DG) is pre-installed in the biaryl that directs metallation as well as controls the stereo-induction step (Scheme 1A).[7] In another approach, similar functions were accomplished by a transient auxiliary that reversibly binds to the aldehyde functionality (Scheme 1B).[8] The latter approach gives the cushion of utilizing catalytic quantity of the chiral ligand cum transient auxiliary over the use of chiral DG attached biaryls.[9] It shall be noted that although both approaches can accommodate diverse functionalizations but can control only the axial chirality. We envisaged developing a catalytic system that can lead to allylation[10] by employing unactivated olefin and can exert simultaneous control on both the axial chirality of the biaryl and the center of chirality at the allylic position. Unlike previous reports on atroposelective allylation using activated allylating reagents, incorporation of an internal olefin as an allyl surrogate at the ortho-position of a biaryl motif itself offers two major challenges: (i) the reactivity should prefer allyl selectivity over styrenyl selectivity, and (ii) control over four stereoisomers arising from two different stereo-environments to selectively form one major diastereoisomer.

A stereoselective transformation relies on a chiral environment predominantly controlled by either a chiral ligand or catalyst.[11] The current diastereoselective transformation to control two distant stereo-environments mandates a judicious choice of metal-ligand system that should aptly fit for the convergence of multiple stereoisomers into a single stereoisomer starting from a racemic biaryl substrate. When controlling two simultaneous stereo-induction, the "combinatorial ligand model" that involves mixing of more than one chiral ligands may become beneficial.[12] In a dual ligand system comprising L_a and L_b ligands, hetero-metal-ligand complexes (ML_aL_b) can form along with corresponding homo-metal-complexes (ML_aL_a or ML_bL_b) depending on the availability of the coordination site of a transition metal and the denticity of the ligand. In many cases it has been observed that hetero-metal-ligand complex plays a key role in the stereo-induction process to obtain an elevated stereoselectivity.[12b,c] Despite its enormous potential, the major focus of such approaches has been on one prochiral center or specifically on center, or axis or plane of chirality

[*] T. Bhattacharya, S. Ghosh, S. Dutta, Dr. S. Guin, A. Ghosh, Prof. R. B Sunoj, Prof. D. Maiti
Department of Chemistry, Indian Institute of Technology Bombay
Powai, Mumbai—400076 (India)
E-mail: sunoj@chem.iitb.ac.in
dmaiti@iitb.ac.in
Prof. H. Ge
Department of Chemistry and Biochemistry, Texas Tech University
Lubbock, TX 79409–1061 (USA)
E-mail: haibo.Ge@ttu.edu

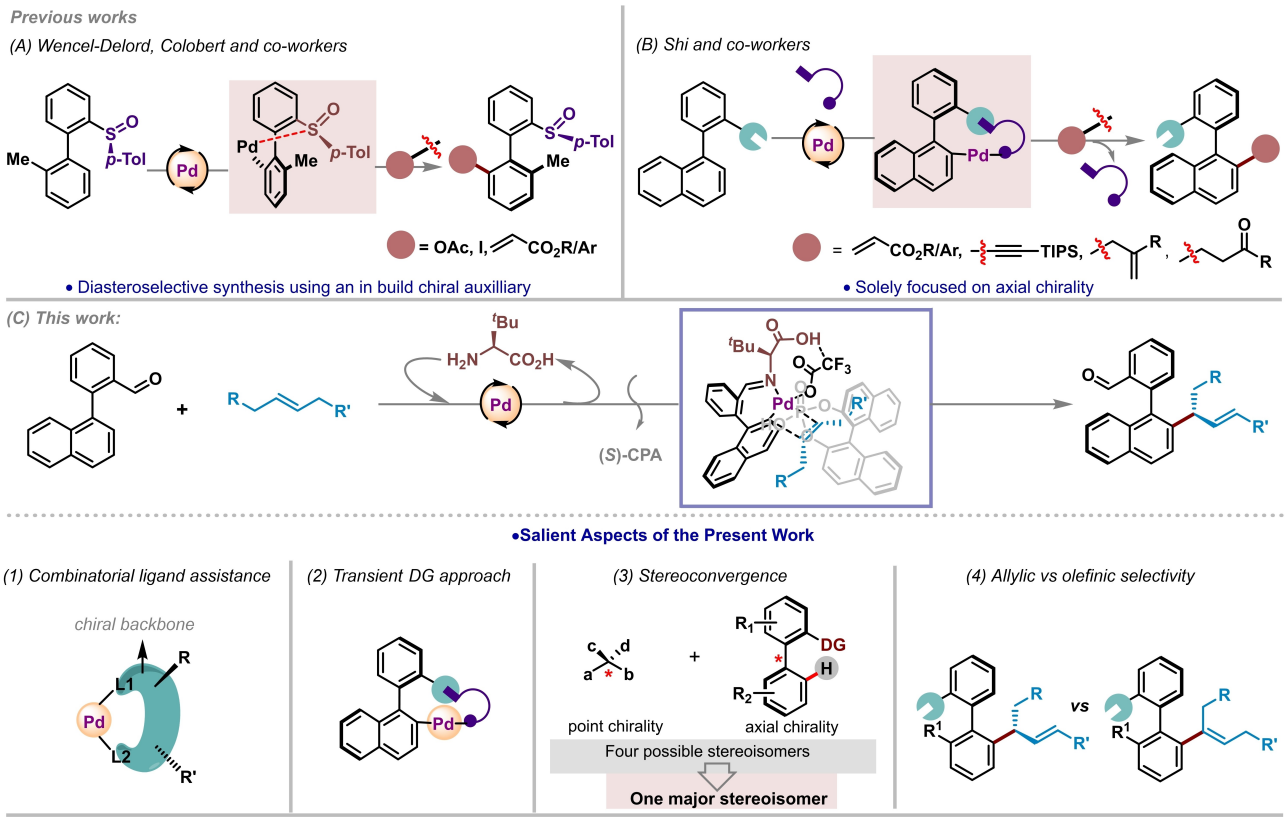

Scheme 1. Ligand assisted stereoselective C–H functionalization.

of a particular substrate.[12b,c] The use of a combinatorial ligand system for stereo-induction at two distant positions has been an unexplored venture in asymmetric C–H functionalizations. This is likely due to the undesirable formation of various diastereoisomers leaving little room for stereocontrol making only a handful of work on this concept till date.[13] In this regard, we have developed the first ever transformation that uses a combinatorial ligand assistance to effectuate Pd-catalyzed atroposelective *o*-allylation of biaryls and is effective in controlling both axis and center of chirality (Scheme 1C).

Results and Discussion

Optimization of the Reaction Conditions

With the objective of accomplishing a diastereoselective functionalization utilizing a chiral transient auxiliary, a preliminary reaction was attempted between the biaryl aldehyde (**1a**) and ethyl trans-3-hexenoate (**2a**) as an allyl source. The reaction was executed in the presence of $Pd(OAc)_2$ catalyst with a mono-ligand system comprising of L-*tert*-leucine (**L1**) in a DCE/AcOH (v/v 4:1) solvent media. The *α*-amino acid ligand **L1** was envisaged to act as the bidentate chiral transient DG ($\mathbf{CT_{DG}}$) and have a simultaneous control over both the axial chirality at the biaryl and the center chirality in the allylic system. Intriguingly, the catalytic system afforded the allylic product **3a** exclusively without any trace of the olefinic product. Noteworthy, for the unsymmetrical internal olefin **2a**, the *β*-hydride elimination to form the olefinic bond in the product is favored towards the ester terminus over the alkyl side. However, the yield (25%) and the level of stereo-induction (*ee* 70%, dr 4:1) exhibited by the ligand **L1** was low. To improve on the yield and stereoselectivity, several variants of *α*-amino acids (**L2**–**L10**) were tested, all of which afforded inferior results in comparison to **L1** (Table 1). Further, the *α*-amino acids were converted to their corresponding amino oxazolines and employed as the chiral transient auxiliary (**L11**–**L14**); albeit found ineffective in promoting the diastereoselective allylation. Subsequently, the amide variants of amino acids (**L15**–**L17**), previously known as effective $\mathbf{CT_{DG}}$,[14] were tested but found unsuitable to augment the stereoselectivity. Additionally, a di-peptide ligand **L18** having two stereo-centers was employed to scrutinize its effect on both the possible proximal axial and distal center chirality in the desired product.[15] Even the dipeptide ligand **L18** failed to have any significant effect in improving the yield or stereoselectivity. The failure of the mono-ligand system in delivering the desired stereo-induction at the allylated product 3a led us to resort to the combinatorial ligand approach. The importance of ligand **L1** as the $\mathbf{CT_{DG}}$ to impart the axial chirality is obvious in this transformation. Thus, to have a simultaneous control of the center of chirality by an additional ligand, we expected that a BINOL-derived chiral phosphoric acid

Table 1: Ligand screening for stereoselective *o*-allylation.[a]

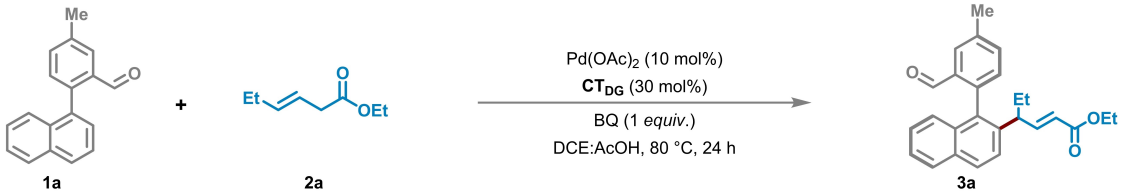

(a) Studies with single ligand

Entry	CT_{DG}	Yield (%)[b]	ee[d]	dr[c]
1	L1	25	70	4:1
2	L2	15	50	1:1
3-7	L3-L7	no product	--	--
8	L8	10	42	1:1
9-10	L9-L10	no product	--	--
11-14	L11-L14	no product	--	--
15	L15	66	40	5:1
16	L16	50	51	5:1
17	L17	no product	--	--
18	L18	30	26	5:1
19-24	L19-L24	no product	--	--

(b) Combinatorial ligand approach

Entry	CT_{DGs}	Yield (%)	ee	dr
25	L1+L19	32	93	9:1
26	L1+L20	trace	--	--
27	L1+L21	35	80	5:1
28	L1+L22	43	72	5:1
29	L1+L23	62	77	3:1
30	L1+L24	65	56	2:1
31[e]	L1+L25	15	48	2:1
32[e]	L1+L26	3	60	1.5:1

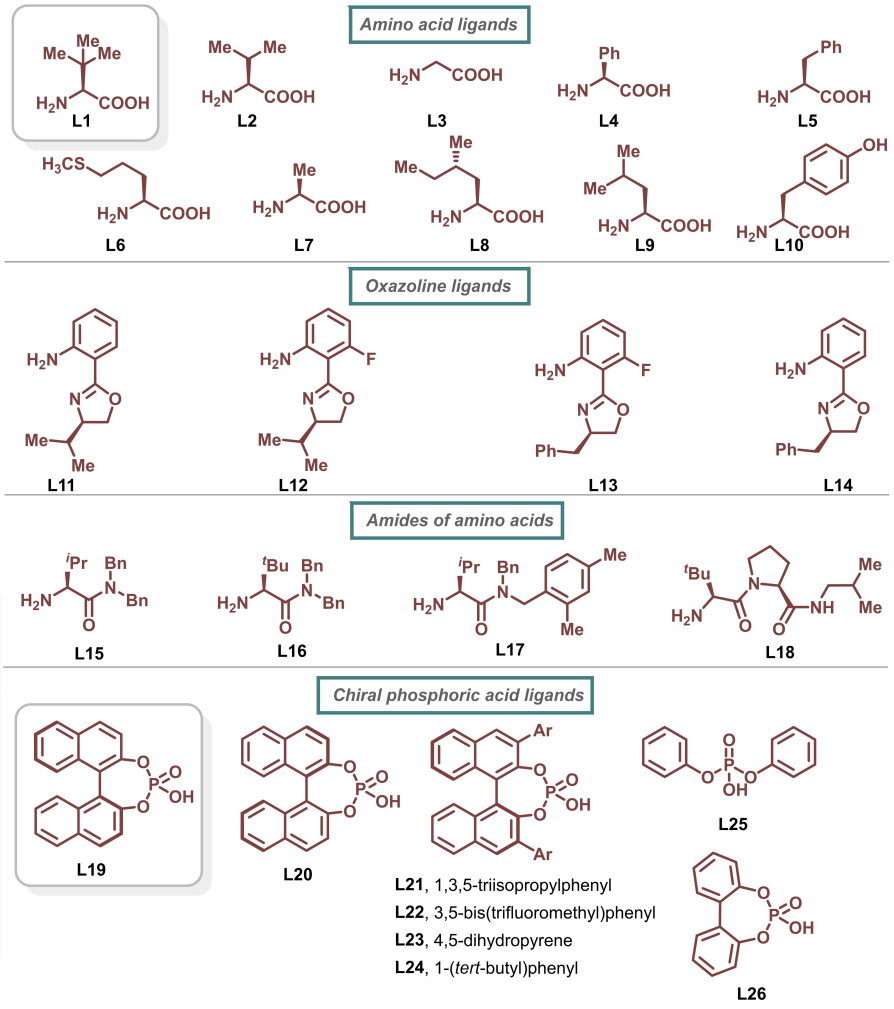

[a]Reactions were performed on a 0.05 mmol scale using solvent DCE:AcOH (0.5 mL/0.0.05 mmol of **1a**) and 3 *equiv.* of **2a**, for a 24 h period at 80 °C.[b]Determined by ^{1}H NMR spectroscopy of the crude reaction mixture using 1,3,5 –trimethoxy benzene (TMB) as internal standard.[c]The branched/linear ratio and the diastereoselectivity [(*Sa,R*)-**3a**/(*Sa,S*)-**3a**] were also determined by ^{1}H NMR on the reaction crude.[d]Determined by chiral HPLC analysis.[e] These reactions were run with the substrate **1e**.

might influence the stereochemistry at the chiral center and hence could enhance the overall stereoselectivity.[16] Interestingly, a simple (*S*)-(+)-1,1-binaphthyl-2,2-diyl hydrogenphosphate (**L19**) drastically improved the stereoinduction to 93 % *ee* with 11:1 dr when used in conjunction with **L1**, thus befitting our hypothesis. Noteworthy, the (*R*)-form of **L19** i.e., **L20** gave only traces of the product indicating how the involvement of a matched ligand-pair is necessary to execute double stereo differentiation in the product. Generally, chiral phosphoric acids (CPA) with bulky substituents at the 3,3′ positions impact the enantioselectivity, although variability exists between different systems to the extent of shutting down the reaction due to steric crowding.[16e] In this case also we observed that no other CPA derivatives **L21**–**L24** were able to improve the yield or stereoselectivity further. On the other hand, we further checked **L25** and **L26** with one of our highest yielding substrate **1e** to clarify whether a rigid conformation of the axis is necessary or if just conformational adjustments in the phosphoric acid frame could yield related optimal results. However, we observed a significant decrease in yield and stereoselectivity in both these cases (Table 1, entry 31 and 32) suggesting that a binaphthyl phosphoric acid is crucial for the present reaction. Worth mentioning that **L19** solely was unable to

deliver **3a**, which alternatively confirms the necessity of a free amine group in **L1** ligand for a facile in situ imine formation that performs the dual role of DG and axial chiral control. Further optimization of other reaction parameters led to the combination of $Pd(TFA)_2$/**L1**+**L19**/p-benzoquinone (BQ)/AcOH at 80 °C for 24 hours which yielded the diastereoselective allylated product **3a** in synthetically useful yield and high stereo-selectivity (see detailed optimization in the Supporting Information).

Substrate Scope

The attainment of the optimal conditions was subsequently followed by the execution of the diastereoselective C–H allylation on different biaryls (Table 2). Gratifyingly, the biaryls could be selectively allylated with high diastereoselectivity whilst generating the center and axial chiralities upon reaction with the internal olefin **2a**. Initially, the substitution at the top aryl ring was varied, and with an electron-withdrawing *meta*-F-substituent with respect to the aldehyde group, moderate yields of the allylated product **3b** was obtained in excellent diastereoselectivity (dr 18:1) and enantioselectivity (*ee* 94 %). A similar stereoselectivity was observed in the allylated product **3c** having F-substituent at the *para*-position to the aldehydic group. Also, with a Cl-substituent, the transformation led to the product **3d** with high stereoselectivity (dr 14:1; *ee* 96 %). However, with the highly electron-rich di-OMe substituent at the aryl ring, even though the yield of the allylated product **3e** was high, the diastereoselectivity was found to be moderate (dr 5:1; *ee* 95 %). Hence the electronic nature and steric environment provided by the substituent at the top aryl ring does influence the yield but it had limited control on the stereoselectivity. Further, when an isopropyl group is present at the *ortho*- position at the bottom ring instead of naphthyl, the yield of the allylated product **3f** decreased considerably while providing high stereoselectivity. A similar trend in stereoselectivity was observed when the top ring was naphthyl and the *para*-position of the bottom arene ring was substituted by either F (**3g**) or OMe (**3h**). A slight decrease in yield was observed when compound **3g** was synthesized in 0.5 mmol scale however the stereochemistry was retained almost intact in the final product (Table 2). It may be noted that in either case second allylation occurred at the other available *ortho* position. Even an attempt for sequential allylation failed which implies the lack of planarity between the transient DG and the other *ortho*-C–H bond due to atropisomerism from the first step does not allow the second C–H metalation (see Supporting Information, page S27). Different variants of the unactivated internal olefins were then attempted towards the diastereoselective allylation with biaryl aldehydes using the chiral transient auxiliary (Table 2). The reaction between methyl pent-3-ene-1-oate (**2b**) with the biaryl aldehyde **1a** afforded the desired allylated product **3i** in synthetically useful yields and diastereoselectivity. The same internal olefin **2b** with the acenaphthene containing biaryl aldehyde gave highly diastereoselective allylated product **3j**. The formation of the allylated product and the absolute configuration for axial (*S*-isomer) and point (*R*-isomer) chirality has been further confirmed by X-ray crystallography (**CCDC 2130315**).[17] It is to be noted that the configuration for the other allylated products have been designated analogously based on the crystal structure obtained. An instance of stereo divergence was observed when the other stereoisomer of compound **3j** was formed in the presence of D-*tert*-leucine and **L20** with −92 % *ee* where the product with opposite configuration **3j′** i.e., *R*-configuration of the chiral axis and *S*-configuration at the center of chirality were observed. With the 4-phenyl substituted naphthyl containing biaryl aldehyde excellent stereoselectivity for the axial and center of chirality was obtained for product **3k**. With a butyl protected derivative of hex-3-ene-1-oic acid, the transformation was found to be efficient in delivering highly stereoselective allylated product **3l** with the biaryl aldehyde **1c**. The protocol was then conducted on benzyl protected hexenoic acid with biaryl aldehydes **1b**, **1c** and **1d** and in all cases moderate yields of respective allylated products (**3m**–**3o**) bearing high level of axial and center of chiralities were obtained. Apart from simple benzyl ester, *para*-tolyl benzyl ester (**3p**) also yielded the desired product with synthetically useful yield and stereoselectivity. Interestingly, long chain fatty acids e.g., oleic acid derivatives where the internal double bond encumbered by long aliphatic chains from both sides, also afforded the *E*-selective *o*-allyl product with high enantioselectivity, albeit with a lower diastereoselectivity (**3q**–**3r**). Similar observation was made with the adamantyl acid protected oleyl alcohol (**3s**). Worth mentioning, that despite the unsymmetrical nature of the internal olefin in oleic acid and oleyl alcohol, allylic double bond formation occurred preferably at the functional group containing terminal. Further, unbiased aliphatic internal alkenes such as 4-octene and 5-decene also delivered the *o*-allyl biaryls (**3t**–**3v**) with high enantioselectivity despite poor diastereoselectivities in them. Unlike others, substrate **1u** is known to undergo kinetic resolution. However, when we checked the HPLC traces of synthesized and unreacted **1u**, both of them showed an enantiomeric ratio of 50:50 which indicated a DKR pathway. This observation could be feasible since at high temperature (at 80 °C the bond rotation could be facile between the two atropisomers). To verify whether it's a KR or DKR pathway, we further isolated two isomers of **1u** i.e. (+) and (−) **1u** by prep HPLC and reacted them separately. At the end, both the isomers were found to retain their initial stereochemistry which indicated a KR pathway for **1u** (see Supporting Information page S27–S28 for detailed HPLC analysis).

Computational Study

To gain mechanistic insights into the $Pd(TFA)_2$ catalyzed atroposelective allylation of racemic biaryls to yield a product with axial as well as center of chirality, density functional theory computations at the SMD(AcOH)/B3LYP-D3/6-31G**,SDD(Pd) level of theory was undertaken.[18] Our computational study is aimed at address-

Table 2: Substrate scope.[a]

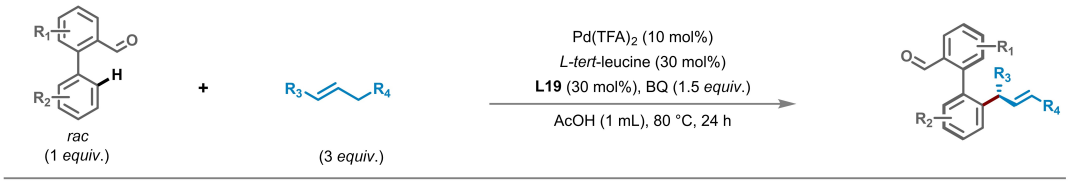

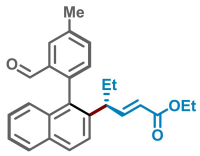

3a, 43%, 11:1 *dr*, 93% *ee*

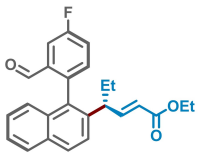

3b, 59%, 18:1 *dr*, 94% *ee*

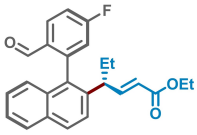

3c, 41%, 19:1 *dr*, 97% *ee*

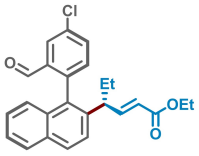

3d, 53%, 14:1 *dr*, 90% *ee*

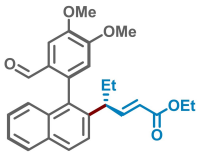

3e, 77%, 5:1 *dr*, 95% *ee*

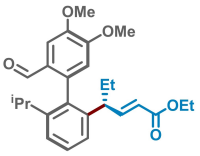

3f, 37%,10:1 *dr*, 94% *ee*

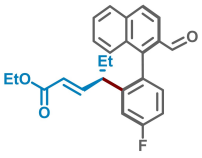

3g, 49%, 3:1 *dr*, 99% *ee*
(0.5 mmol scale, 40%, 3:1 *dr*, 98% *ee*)

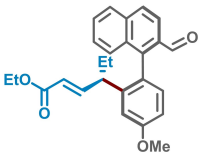

3h, 51%, 3:1 *dr*, 99% *ee*

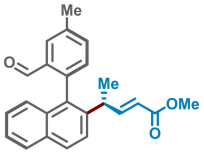

3i, 55%, 12:1 *dr*, 82% *ee*

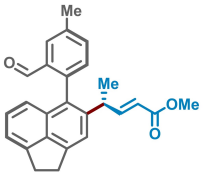

3j, 42%, 10:1 *dr*, 96% *ee*
3j', 38%,10:1 *dr*, -92% *ee*

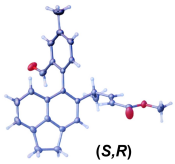

(*S*,*R*)
X-ray structure of 3j
CCDC 2130315

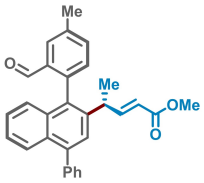

3k, 47%, 10:1 *dr*, 95% *ee*

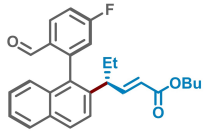

3l, 45%, 20:1 *dr*, 98% *ee*,

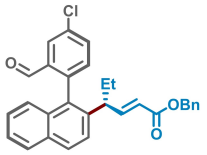

3m, 53%, 12:1 dr, 95% *ee*

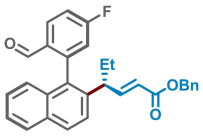

3n, 49%, 30:1 *dr*, 94% *ee*

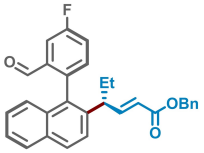

3o, 61%, 19:1 *dr*, 99% *ee*

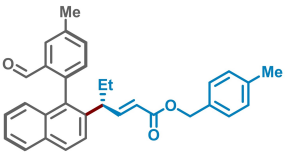

3p, 46%, 10:1 *dr*, 94% *ee*

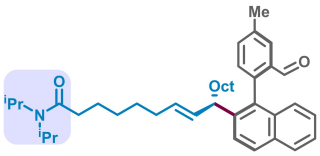

3q, 46%, 2:1 *dr*, 83% *ee*

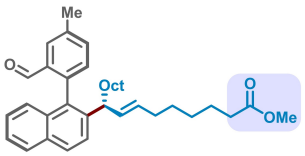

3r, 43%, 2.5:1 *dr*, 87% *ee*

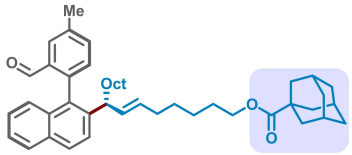

3s, 48%, 3:1 *dr*, 98% *ee*

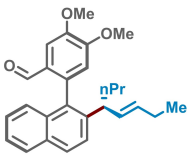

3t[b], 41%, 2:1 *dr*, 85% *ee*

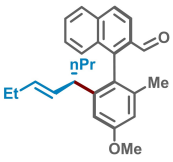

3u[b], 39%, 2:1 *dr*, 96% *ee*
via kinetic resolution

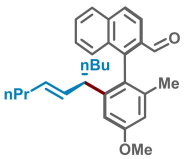

3v[b], 36%, 2:1 *dr*, 75% *ee*
via kinetic resolution

[a]Reactions performed at 0.1 mmol scale in AcOH (1 mL/0.1 mmol of **1**) with 3 *equiv.* of ethyl trans-3-hexenoate for a 24 h period at 80 °C.[b]NaOTf (2 *equiv.*) was added. The dr's were determined by ^{1}H NMR spectroscopy in the crude reaction mixtures. The *ee*'s were determined by chiral HPLC analysis.

ing several important aspects of this reaction, such as a) the identification of the most likely catalytic pathway based on the energetic span, b) the origin of observed stereoselectivity leading to axial and center of chirality, c) the role of chiral auxiliary *L-tert*-leucine in asymmetric induction, d) whether or not the chiral phosphoric acid (CPA) which is used as an

additive is directly involved in the catalytic cycle or the reaction may proceed in the absence of CPA,[19] and e) the origin of low diastereoselectivity observed in the case of unactivated internal olefins. A comprehensive investigation is undertaken where multiple possibilities are considered for each catalytic step to identify the most likely pathway. The results are organized in the following sections; i) generation of the active catalyst and the primary catalytic cycle, ii) the C(sp^2)–H functionalization of the racemic biaryl, iii) migratory insertion step, iv) Gibbs free energy profile, and v) the origin of stereoselectivity. The catalytic cycle in the case of racemic **1e** as the starting substrate can be considered to begin with the formation of a catalyst-substrate complex **4e** as shown in Scheme 2. This Pd-bound aldimine **4e** formed by the action of *L-tert*-leucine on racemic biaryl aldehyde could serve as a potential active catalyst. We envisaged explicit participation of (S_a)-CPA, trifluoroacetate, water, and benzoquinone (BQ) in the generation of this active catalyst species. Apart from the substrate, (S_a)-CPA, water, and BQ might as well bind to Pd(II) through various ligand exchanges.[20] The biaryl aldimine can coordinate to Pd(II) through the N and/or O center, either in a monodentate or a bidentate chelation.[21] The monodentate binding of the substrate through the aldimine *N* is found to be energetically more favorable over the bidentate alternative resulting in the most exoergic species (**4e**) from the precatalyst Pd(TFA)$_2$ (**1**). The additive (S_a)-CPA is incorporated as the counter ion, hydrogen bonded to H_3O^+, in the near vicinity of the substrate (Scheme 2).[21] While detailed discussions on each catalytic step are provided in the subsequent sections, here we focus on the key events. First, the C–H bond activation of the Pd-bound biaryl aldimine can give a palladacycle intermediate **5e**. The migratory insertion of the allyl coupling partner **2a** to the Pd-aryl bond in **5e** through a specific prochiral face can then generate a new stereogenic center in intermediate **7e**. The Pd-alkyl intermediate **7e** can

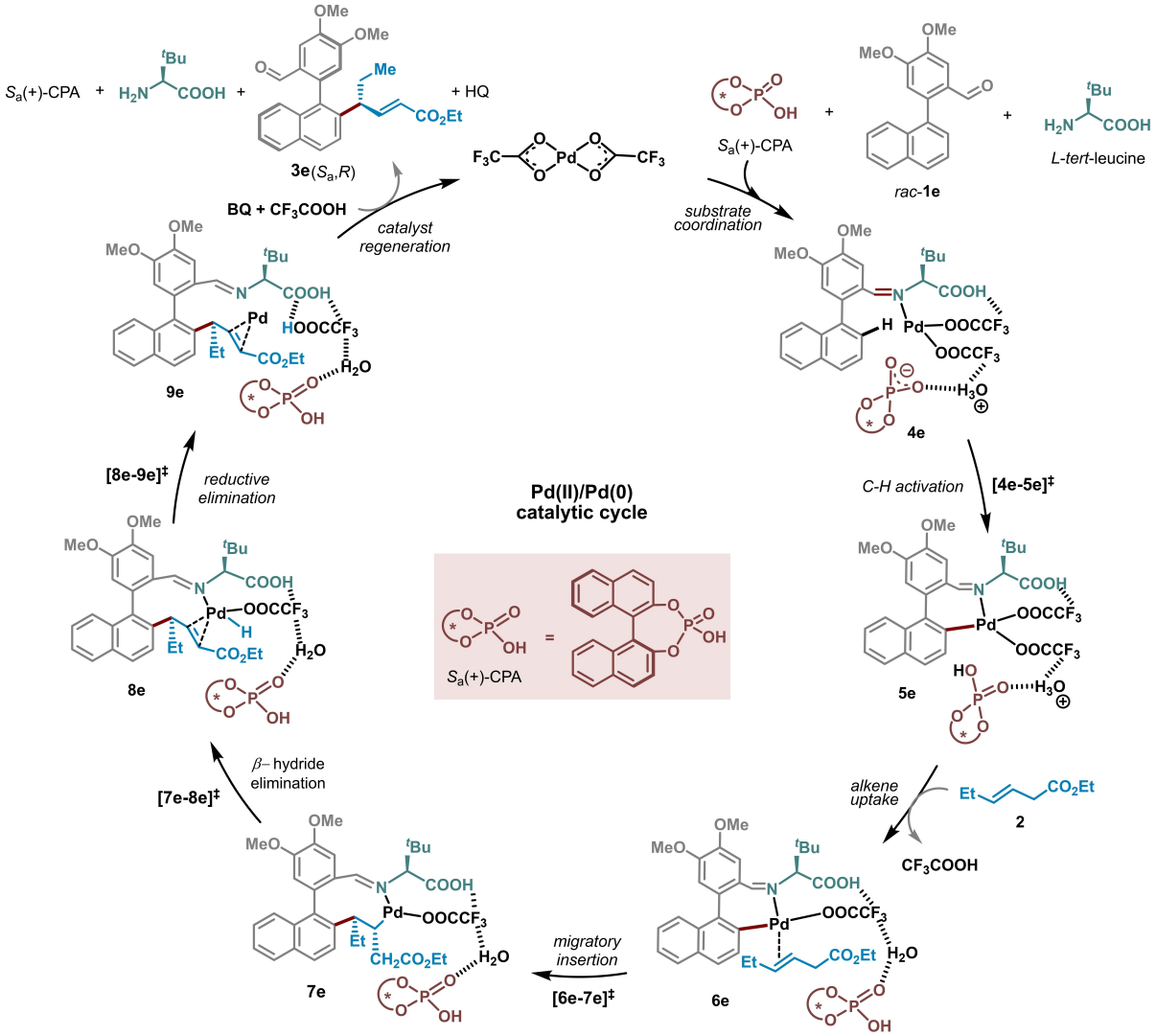

Scheme 2. Mechanistic cycle for the Pd(II)-catalyzed atroposelective allylation of racemic biaryl aldehyde (**1e**) in the presence of *L-tert*-leucine and axially chiral phosphoric acid.

then undergo a β-hydride elimination to give Pd(II)-hydride **8e** and then a reductive elimination can furnish the desired product-catalyst complex **9e**. The oxidation of Pd(0) in **9e** to Pd(II) by benzoquinone (BQ) can help sustain the catalytic cycle. In the first major step of the mechanism, the chiral aldimine moiety serves as the directing group for bringing the Pd center closer to the *ortho* aryl C(sp^2)–H bond enabling the bond activation through a concerted metalation deprotonation (CMD). The ligand involved here could be the Pd-bound trifluoroacetate, or an external base such as the chiral phosphate derived from (S_a)-CPA, or even an unbound trifluoroacetate. Different likely combinations among the available ligands around the Pd(II) center are considered for their involvement in the C–H bond activation.[22] The Gibbs free energy of the transition states for the external phosphate assisted C–H bond activation (**[4e–5e]**‡/**[4c–5c]**‡) is found to be 20–25 kcal/mol more preferred over the corresponding Pd-bound trifluoroacetate-assisted alternative (**[4e′–5e′]**‡/**[4c′–5c′]**‡ as shown in Figure 1a), suggesting a vital role of (S_a)-CPA early on in the mechanism. Given that the starting material **1e**/**1c** participating in the form of corresponding aldimine is racemic, the R_a and S_a enantiomers are expected to show differential reactivity in the presence of (S_a)-CPA. In the (S_a)-CPA assisted pathway, the Gibbs free energy of the C–H bond activation TS **[4e–5e]**‡ for (R_a)-**1e** is found to be 3.0 kcal/mol lower than (S_a)-**1e**, indicating that the R_a enantiomer would react faster than the S_a (Figure 1a). The elementary step barrier, computed with respect to the corresponding pre-reacting complex of TS **[4e–5e]**‡ for the (R_a)-enantiomer is 2.3 kcal/mol lower than that from (S_a)-enantiomer. A similar energetic preference for (R_a)-**1c** over (S_a)-**1c** is noted in the case of racemic **1c** as well (Figure 1a). Such energetic details imply a possible kinetic resolution or even a dynamic kinetic resolution in this catalytic transformation. In view of the kinetic advantage, the (R_a)-configuration of the palladacycle intermediate **5e** is considered as the major intermediate obtained from the C–H bond activation step. An intramolecular proton transfers from H_3O^+ to the Pd-bound trifluoroacetate in **5e** can facilitate a ligand exchange with the alkene **2a**, leading to the formation of a π-complex **6e** with the release of trifluoroacetic acid (Figure 1b). With this, the stage is set for the stereocontrolling migratory insertion via a four membered transition state **[6e–7e]**‡. Two different binding possibilities for the alkene to the Pd(II) center that differ in terms of the relative proximity between the -CO_2Et group of the alkene and (S_a)-CPA are considered. As shown in Figure 1c, in mode-I the -CO_2Et group is closer to the (S_a)-CPA while in mode-II it is farther. Within each of these binding modes, the prochiral face of **2a** involved in the migratory insertion can give rise to four stereochemically distinct transition states, denoted using *re*-I, *si*-I, *re*-II, and *si*-II stereochemical descriptors, as applicable.[23] Here, the *re*/*si* refers to the prochiral face of the alkene carbon of **2a** that forms the new C-C bond with the aryl carbon during the migratory insertion. It should be noted that the configuration of the axially chiral biaryl changes upon going from intermediate **6e** to **7e** due to the change in priority order of the substituents along the chiral axis. The change in the axial configuration effected by the migratory insertion to the *ortho*-position of the biaryl appears like a reversal of configuration in the product as compared to the axial configuration at the beginning of the catalytic cycle.

An important aspect pertaining to the formation of the new chiral center in the product is directly linked to the stereochemical preferences in the migratory insertion step, thus demands careful scrutiny. The mode-I insertion of the alkene (**2a**) to the Pd-aryl bond in through TS **[6e–7e]**‡ is found to be 1.5–2.0 kcal/mol more preferred over that from mode-II binding of (R_a)-**1e**. A similar trend in the energetic preference is also noticed in the case of (S_a)-**1e** for mode-I binding over mode-II by about 4–7 kcal/mol (Figure 2). The migratory insertion TS **[6e–7e]***re*-I‡ involving the *re*-I face in (R_a)-**6e** leading to the (S_a,*R*) product is found to be 1.4 kcal/mol lower than that through the *si*-I face. Interestingly, the transition states for the *re*-I and *si*-I face insertions in the case of the enantiomeric substrate (S_a)-**6e** are about 6–9 kcal/mol higher than that responsible for the formation of the (S_a,*R*) product from (R_a)-**6e**. These data suggest that the most preferred binding of **2a** is through its *re*-I face and a migratory insertion in such a binding mode would lead to the formation of the (S_a,*R*) stereoisomer of the final product. Another important aspect of the transition state models shown in Figure 2 is the explicit participation of the chiral (S_a)-CPA. The fact that the new chiral center is generated via the migratory insertion step, the presence of a chiral inductor such as (S_a)-CPA should be considered desirable. Interestingly, the expulsion of (S_a)-CPA prior to the migratory insertion resulted in transition states 10–20 kcal/mol higher energy as compared to those with a bound (S_a)-CPA molecule.[24] Therefore, the computational investigation demonstrates that the absence of (S_a)-CPA renders the reaction pathway energetically unfavorable, aligning with experimental findings (Table 1). In addition, the product stereoselectivity predicted using such transition states devoid of (S_a)-CPA is also found to be incorrect. The role of (S_a)-CPA in the stereocontrolling migratory insertion manifests in the form of providing access to lower energy pathway as well in controlling the stereochemical outcome of the reaction. In the case of (S_a)-CPA assisted allylation, the Gibbs free energies indicate the exclusive formation of the product bearing the (S_a,*R*) configuration from racemic **1e** involving **[6e–7e]**‡*re*-I as the stereocontrolling TS. Similarly, racemic **1c** is predicted to offer (S_a,*R*) product via **[6c–7c]**‡*re*-I.[25]

On the other hand, the corresponding *si*-I mode of migratory insertion through **[6e–7e]**‡ is found to be 1.4 kcal/mol higher than the *re*-I mode (Figure 1d). Such a difference in TS energies corresponds to a diastereoselectivity of 76 %, which is in good agreement with the experimentally observed diastereomeric ratio (5:1) in favor of the (S_a,*R*) product.[26] The migratory insertion to the *re*-I face is 2.8 kcal/mol lower than the *si*-I face for substrate **1c**, suggesting a *de* of 96 % in concert with our experimental observation (19:1 dr). The application of the energetic span model[27] on the Gibbs free energy profile revealed that the palladacycle intermediate **5e** is the turn-over determining

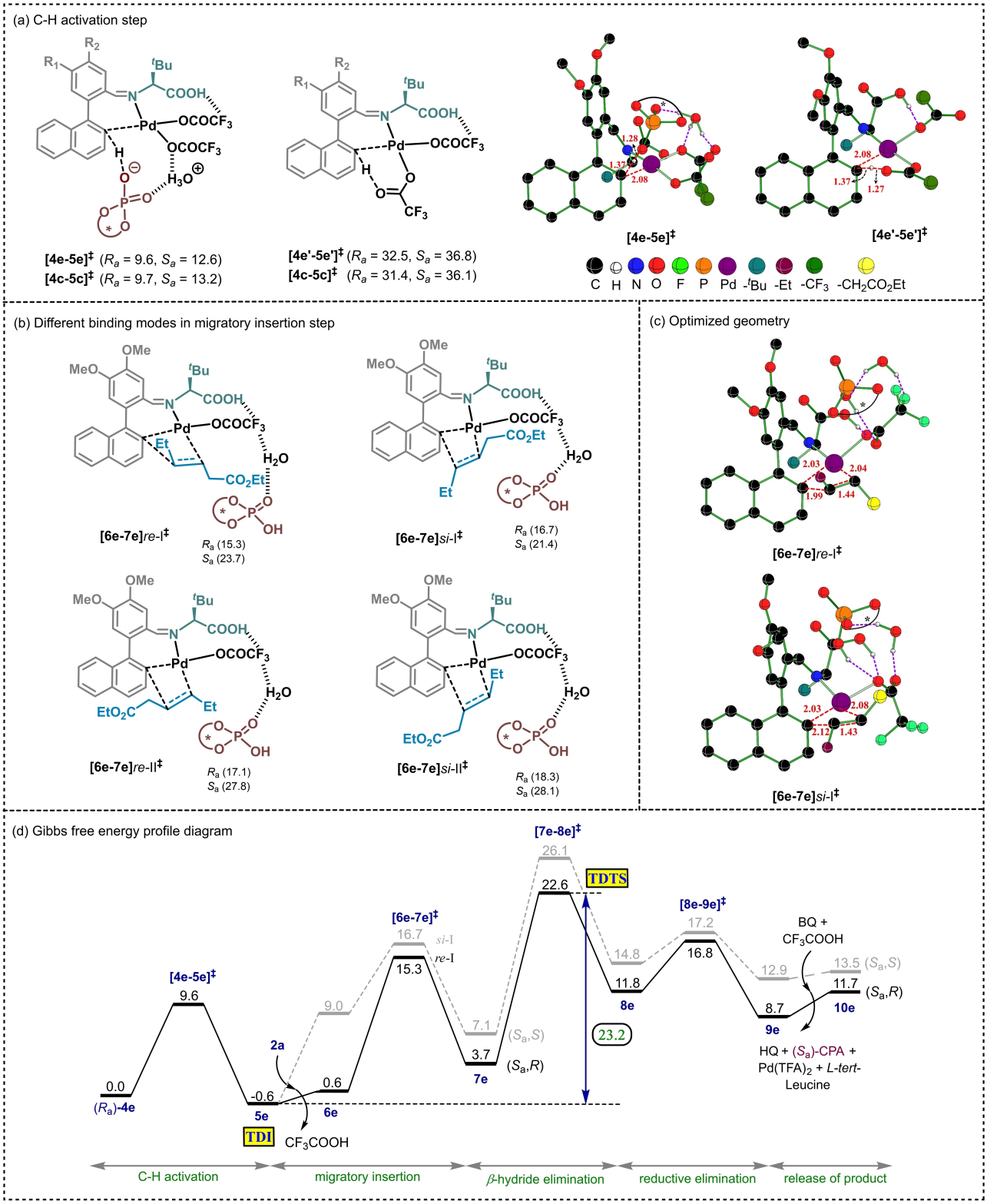

Figure 1. Theoretical calculations: (a) Optimized geometries of C(sp^2)-H bond activation transition state and the corresponding relative Gibbs free energies (in kcal/mol given in parentheses) with respect to the respective catalyst-substrate complex (R_a)-**4e/4c**. Distances are in Å and hydrogen bonding interactions involving H_3O^+ ion are shown using violet-colored dotted lines. (b) Schematic representation of different modes of migratory insertion of alkene to the Pd-aryl bond in TS **[6e–7e]**‡. Relative Gibbs free energies (in kcal/mol) with respect to (R_a)-**4e** are provided in parentheses. (c) A simplified depiction of the optimized geometries of mode-I migratory insertion transition states. (d) The Gibbs free energy profile (in kcal/mol) for the Pd-catalyzed atroposelective allylation of racemic biaryl (**1e**). For sake of improved clarity only (R_a)-**1e** is shown as a representative case.

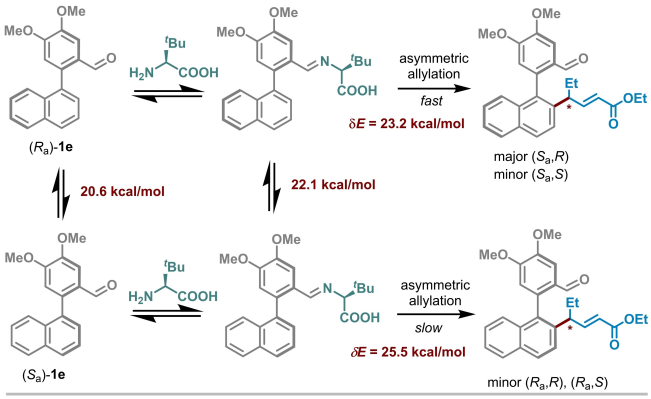

Figure 2. Schematic representation of the probable reaction pathway for the Pd-catalyzed atroposelective allylation of racemic biaryl (**1e**).

intermediate (TDI) and the β-hydride elimination transition state **[8e–9e]**‡ is the turn-over determining transition state (TDTS) of the catalytic cycle (Figure 1d). The energy difference between the TDTS and TDI is the energetic span (δE), which is found to be 23.2 kcal/mol with a turnover frequency (TOF) of $2.38\times10^{-2}\ s^{-1}$ at 353.15 K.[28] The δE value is suggestive of an effective catalytic transformation at 80 °C, which is in conformity with the reaction conditions employed.

Another interesting discernible aspect from the Gibbs free energy profile (Figure 1d) is that the C–H activation step is likely more reversible and not the turnover determining step.[29] To verify the reversibility of the C–H activation step, additional experiments were performed using d_1-HFIP solvent. In the presence of d_1-HFIP, significant amount of deuterium exchange was observed (Scheme 3), where both the accessible *ortho*-C–H bonds got deuterated. This observation implies that the C–H activation step might be reversible in nature.[30]

Dynamic Kinetic Resolution (DKR)

The yield of the reaction in the case of substrate **1e** was found to be 77 %, indicating that both the enantiomers of the racemic starting material are converted into the final product. This observation can be reconciled by considering different mechanistic scenarios as shown in Figure 2. The most likely possibility is a dynamic kinetic resolution (DKR) wherein one enantiomer of **1e** interconverts to another, due

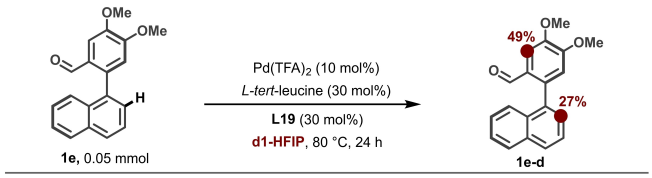

Scheme 3. Reversibility experiment. [a]Reaction was performed at 0.05 mmol scale in d1-HFIP (0.5 mL/0.05 mmol of **1e**) for a 24 h period at 80 °C.

to the difference in their reactivities. Interestingly, the barrier to interconversion of (S_a)-**1e** to (R_a)-**1e** is found to be 20.6 kcal/mol, which is 4.9 kcal/mol lower than the energetic span in the (S_a)-**1e** catalytic pathway (Figure 2).[28] Similarly, the (S_a)-**1e** to (R_a)-**1e** interconversion barrier in the form of the corresponding aldimine is also found to be energetically more feasible (22.1 kcal/mol) than the energetic span found in the (S_a)-**1e** catalytic pathway. Thus, the asymmetric allylation of (R_a)-**1e** can take place through a preferred natural route to the desired product whereas a rapid interconversion of (S_a)-**1e** to (R_a)-**1e** engages (S_a)-**1e** in the reaction. Such DKR helps in accessing the desired biaryl product **3e** with high enantio- and diastereo-selectivity. Similar to substrate **1e**, the barrier for the (S_a)-**1c** to (R_a)-**1c** interconversion is about 4 kcal/mol lower than the energetic span found involving the (S_a)-**1c** catalytic pathway, alluding to a DKR pathway.[31]

Reaction with Unactivated Olefin

Another observation that invited our attention was a drastic lowering of diastereoselectivity when experiments were conducted with an unactivated olefin such as 4-octene as compared to alkene **2a** bearing an ethyl ester group. Using our understanding about the transition state for the stereocontrolling migratory insertion step involving substrate **1e** and alkene **2a**, we have considered the *si*-I and *re*-I modes of additions of the unactivated 4-octene.[32] As anticipated, the unactivated alkene exhibits higher barrier (by about 8–9 kcal/mol) over the activated alkene. The elementary step barriers for the migratory insertion for the *re*-I and *si*-I TSs with 4-octene are respectively found to be 21.1 and 20.9 kcal/mol. Furthermore, the energy difference between lower energy diastereomeric *re*-I and *si*-I TSs is reduced from 2.8 kcal/mol for alkene **2a** to 0.3 kcal/mol for 4-octene. Therefore, the computed diastereoselectivity of the reaction involving 4-octene is as low as 21 %, in agreement with the low observed diastereoselectivity in our experiments (*dr* 2:1).

Origin of Stereoselectivity

The stereocontrolling transition states are anaylsed using the activation strain model[33] to gather additional insights into the factors responsible for the origin of the center of chirality. We have probed the effect of distortion and interaction between the reaction partners as they move from their respective ground state to the transition state geometry.[34] The sum of the distortion energies for each of the reacting partners at the transition state is found to be higher by 16.3 kcal/mol for the lower energy **[6e–7e]***re*-I‡ as compared to the higher energy diastereomeric counterpart **[6e–7e]***si*-I‡. On the other hand, the stabilizing interaction energy between these distorted fragments is found to be lower by 19.5 kcal/mol in [6e–7e]*re*-I‡ than that in **[6e–7e]***si*-I‡. The net effect of these opposing factors is found to be in favor of the lower energy **[6e–7e]***re*-I‡ transition state. The

presence of more effective interactions between the chiral (S_a)-CPA, substrate, and the catalyst can therefore be regarded as the major contributing factor rendering the migratory insertion to the *si*-I prochiral face more preferred over that to the *re*-I face of the olefin. Similarly, the origin of axis of chirality induced in the C–H activation step could be understood based the relative distortion and interaction.[32] The total distortion energy is found to be 1.9 kcal/mol higher in **[4e–5e]**$_S^{\ddagger}$ than that in **[4e–5e]**$_R^{\ddagger}$. Also, the stabilizing interaction energy between these distorted fragments is higher by 1.5 kcal/mol in the **[4e–5e]**$_S^{\ddagger}$, thereby resulting in an overall stabilization of the lower energy **[4e–5e]**$_R^{\ddagger}$. The interactions between the substrate and the (S_a)-CPA catalyst fragment can therefore be considered to play a crucial role in rendering **[4e–5e]**$_R^{\ddagger}$ as the lower energy transition state. The above analysis indicates that the substrate bound chiral auxiliary *L-tert*-leucine influences the axial chirality of the final product.

Conclusion

In summary we have developed a protocol to synthesize diastereoselective allylation of axially chiral biaryls. Cooperative assistance by L-*tert*-leucine and *S*(+) chiral phosphoric acid offered a highly stereoselective pathway to the product. An array of substituted biaryl aldehydes were tolerated under the reaction condition. High stereoselectivity was observed even when a long chain aliphatic fatty acid derivatives were used as the allyl source. Among the various steps involved in the catalytic cycle, the β-hydride elimination is found to be the turn-over determining transition state and the palladacycle intermediate formed via the C–H bond activation is the turn-over determining intermediate. Enrichment in favor of (R_a)-axial chiral product from the racemic starting material is found to depend on the chiral auxiliary L-*tert*-leucine, which preferentially engages the (R_a)-enantiomer in the C–H bond activation over the corresponding (S_a)-enantiomer. In the ensuing step, the migratory insertion of the Pd-bound alkene through its *re* prochiral face is found to be energetically most preferred leading to the (S_aR) product, bearing an axis and a center of chirality.

Author Contributions

D.M. conceived the concept. T.B., S.D. S.G. and A.G. performed the experiments. S.G. and R.B.S. performed the computational studies. T.B. thanks UGC-India, A.G. and S.G. thanks CSIR-Indian for the financial assistance. The manuscript was written through contributions of all authors. All authors have given approval to the final version of the manuscript.

Acknowledgements

Financial support from the Indian Science and Engineering Research Board(SERB) (CRG/2022/004197 to D.M.), University Grants Commission (fellowship to T.B.) and CSIR-India (fellowship to S.G.) is gratefully acknowledged. H. G. acknowledges NSF (CHE-2029932), the Robert A. Welch Foundation (D-2034-20230405), and Texas Tech University for financial support. Authors are thankful for the financial support from Bristol Myers Squibb USA.

Conflict of Interest

The authors declare no conflict of interest.

Data Availability Statement

The data that support the findings of this study are available in the supplementary material of this article.

Keywords: Atroposelective · Chiral Phosphoric Acids · Co-Operative Assistance · DFT Analysis · Transient DG

[1] a) L. Ackermann, *Org. Process Res. Dev.* **2015**, *19*, 260–269; b) D. Basu, S. Kumar, S. S. V, R. Bandichhor, *J. Chem. Sci.* **2018**, *130*, 1–11; c) T. Cernak, K. D. Dykstra, S. Tyagarajan, P. Vachal, S. W. Krska, *Chem. Soc. Rev.* **2016**, *45*, 546–576; d) H. M. Davies, D. Morton, *ACS Cent. Sci.* **2017**, *3*, 936–943; e) L. Guillemard, N. Kaplaneris, L. Ackermann, M. J. Johansson, *Nat. Chem. Rev.* **2021**, *5*, 522–545; f) R. Jana, H. M. Begam, E. Dinda, *Chem. Commun.* **2021**, *57*, 10842–10866; g) J. D. Lasso, D. J. Castillo-Pazos, C.-J. Li, *Chem. Soc. Rev.* **2021**, *50*, 10955–10982; h) M. Seki, *Org. Process Res. Dev.* **2016**, *20*, 867–877; i) S. K. Sinha, S. Guin, S. Maiti, J. P. Biswas, S. Porey, D. Maiti, *Chem. Rev.* **2022**, *122*, 5682–5841; j) J. Wencel-Delord, F. Glorius, *Nat. Chem.* **2013**, *5*, 369–375; k) J. Yamaguchi, A. D. Yamaguchi, K. Itami, *Angew. Chem. Int. Ed.* **2012**, *51*, 8960–9009.

[2] a) R. Noyori, *Angew. Chem. Int. Ed.* **2002**, *41*, 2008–2022; b) C. Zheng, S.-L. You, *RSC Adv.* **2014**, *4*, 6173–6214; c) K. Liao, S. Negretti, D. G. Musaev, J. Bacsa, H. M. Davies, *Nature* **2016**, *533*, 230–234; dX. Yu, Z.-Z. Zhang, J.-L. Niu, B.-F. Shi, *Org. Chem. Front.* **2022**, *9*, 1458–1484.

[3] a) T. G. Saint-Denis, R.-Y. Zhu, G. Chen, Q.-F. Wu, J.-Q. Yu, *Science* **2018**, *359*, eaao4798; b) Q. Zhang, B.-F. Shi, *Acc. Chem. Res.* **2021**, *54*, 2750–2763; c) S. Cheng, Q. Li, X. Cheng, Y. M. Lin, L. Gong, *Chin. J. Chem.* **2022**, *40*, 2825–2837; d) B.-B. Zhan, L. Jin, B.-F. Shi, *Trends Chem* **2022**, *4*, 220–235, DOI: 10.1016/j.trechm.2021.12.005.

[4] a) T. K. Achar, S. Maiti, S. Jana, D. Maiti, *ACS Catal.* **2020**, *10*, 13748–13793; b) X. Bao, J. Rodriguez, D. Bonne, *Angew. Chem. Int. Ed.* **2020**, *59*, 12623–12634.

[5] a) P. Wipf, E. M. Skoda, A. Mann, in *The practice of medicinal chemistry*, Elsevier, Amsterdam, **2015**, pp. 279–299; b) Q. Yue, B. Liu, G. Liao, B.-F. Shi, *ACS Catal.* **2022**, *12*, 9359–9396.

[6] a) J. Wencel-Delord, A. Panossian, F. Leroux, F. Colobert, *Chem. Soc. Rev.* **2015**, *44*, 3418–3430; b) G. Liao, T. Zhou, Q.-J. Yao, B.-F. Shi, *Chem. Commun.* **2019**, *55*, 8514–8523; c) G. Liao, T. Zhang, Z.-K. Lin, B.-F. Shi, *Angew. Chem. Int. Ed.* **2020**, *59*, 19773–19786; d) B.-F. Shi, F. Colobert, *Chem Catal.* **2021**, *1*, 485–487; e) C.-X. Liu, W.-W. Zhang, S.-Y. Yin, Q. Gu, S.-L. You, *J. Am. Chem. Soc.* **2021**, *143*, 14025–14040; f) J. K. Cheng, S.-H. Xiang, S. Li, L. Ye, B. Tan, *Chem. Rev.* **2021**, *121*, 4805–4902; g) D. Chandra, U. Sharma, *Org. Biomol. Chem.* **2021**, *19*, 4014–4026; h) J. A. Carmona, C. Rodríguez-Franco,

R. Fernández, V. Hornillos, J. M. Lassaletta, *Chem. Soc. Rev.* **2021**, *50*, 2968–2983.

[7] a) T. Wesch, A. Berthelot-Brehier, F. R. Leroux, F. Colobert, *Org. Lett.* **2013**, *15*, 2490–2493; b) T. Wesch, F. R. Leroux, F. Colobert, *Adv. Synth. Catal.* **2013**, *355*, 2139–2144; c) C. K. Hazra, Q. Dherbassy, J. Wencel-Delord, F. Colobert, *Angew. Chem.* **2014**, *126*, 14091–14095; d) Q. Dherbassy, G. Schwertz, C. K. Hazra, T. Wesch, J. Wencel-Delord, F. Colobert, *Phosphorus Sulfur Silicon Relat. Elem.* **2015**, *190*, 1339–1351; e) Q. Dherbassy, G. Schwertz, M. Chesse, C. K. Hazra, J. Wencel-Delord, F. Colobert, *Chem. Eur. J.* **2016**, *22*, 1735–1743; f) P. Schmitz, M. Malter, G. Lorscheider, C. Schreiner, A. Carboni, S. Choppin, F. Colobert, A. Speicher, *Tetrahedron* **2016**, *72*, 5230–5237.

[8] a) Q. J. Yao, S. Zhang, B. B. Zhan, B. F. Shi, *Angew. Chem.* **2017**, *129*, 6717–6721; b) G. Liao, B. Li, H. M. Chen, Q. J. Yao, Y. N. Xia, J. Luo, B. F. Shi, *Angew. Chem. Int. Ed.* **2018**, *57*, 17151–17155; c) G. Liao, Q. J. Yao, Z. Z. Zhang, Y. J. Wu, D. Y. Huang, B. F. Shi, *Angew. Chem.* **2018**, *130*, 3723–3727; d) H.-M. Chen, S. Zhang, G. Liao, Q.-J. Yao, X.-T. Xu, K. Zhang, B.-F. Shi, *Organometallics* **2019**, *38*, 4022–4028; e) G. Liao, H. M. Chen, Y. N. Xia, B. Li, Q. J. Yao, B. F. Shi, *Angew. Chem.* **2019**, *131*, 11586–11590; f) S. Zhang, Q.-J. Yao, G. Liao, X. Li, H. Li, H.-M. Chen, X. Hong, B.-F. Shi, *ACS Catal.* **2019**, *9*, 1956–1961.

[9] a) J. I. Higham, J. A. Bull, *Org. Biomol. Chem.* **2020**, *18*, 7291–7315; b) N. Goswami, T. Bhattacharya, D. Maiti, *Nat. Chem. Rev.* **2021**, *5*, 646–659.

[10] a) S. Maity, P. Dolui, R. Kancherla, D. Maiti, *Chem. Sci.* **2017**, *8*, 5181–5185; b) T. K. Achar, X. Zhang, R. Mondal, M. Shanavas, S. Maiti, S. Maity, N. Pal, R. S. Paton, D. Maiti, *Angew. Chem.* **2019**, *131*, 10461–10468; c) A. Baccalini, S. Vergura, P. Dolui, S. Maiti, S. Dutta, S. Maity, F. F. Khan, G. K. Lahiri, G. Zanoni, D. Maiti, *Org. Lett.* **2019**, *21*, 8842–8846; d) S. Dutta, T. Bhattacharya, D. B. Werz, D. Maiti, *Chem* **2021**, *7*, 555–605.

[11] a) K. Muñiz, C. Bolm, *Chem. Eur. J.* **2000**, *6*, 2309–2316; b) A. Pfaltz, W. J. Drury III, *Proc. Natl. Acad. Sci. USA* **2004**, *101*, 5723–5726; c) S. P. Flanagan, P. J. Guiry, *J. Organomet. Chem.* **2006**, *691*, 2125–2154.

[12] a) K. Mikami, S. Matsukawa, T. Volk, M. Terada, *Angew. Chem. Int. Ed.* **1997**, *36*, 2768–2771; b) M. T. Reetz, *Angew. Chem. Int. Ed.* **2001**, *40*, 284–310; c) D. Peña, A. J. Minnaard, J. A. Boogers, A. H. de Vries, J. G. de Vries, B. L. Feringa, *Org. Biomol. Chem.* **2003**, *1*, 1087–1089.

[13] A. Romero-Arenas, V. Hornillos, J. Iglesias-Sigüenza, R. Fernández, J. López-Serrano, A. Ros, J. M. Lassaletta, *J. Am. Chem. Soc.* **2020**, *142*, 2628–2639.

[14] a) H. Park, P. Verma, K. Hong, J.-Q. Yu, *Nat. Chem.* **2018**, *10*, 755–762; b) H. Song, Y. Li, Q. J. Yao, L. Jin, L. Liu, Y. H. Liu, B. F. Shi, *Angew. Chem.* **2020**, *132*, 6638–6642.

[15] a) E. R. Jarvo, S. J. Miller, *Tetrahedron* **2002**, *58*, 2481–2495; b) E. A. C. Davie, S. M. Mennen, Y. Xu, S. J. Miller, *Chem. Rev.* **2007**, *107*, 5759–5812.

[16] a) D. Parmar, E. Sugiono, S. Raja, M. Rueping, *Chem. Rev.* **2014**, *114*, 9047–9153; b) P. S. Wang, H. C. Lin, Y. J. Zhai, Z. Y. Han, L. Z. Gong, *Angew. Chem. Int. Ed.* **2014**, *53*, 12218–12221; c) S.-B. Yan, S. Zhang, W.-L. Duan, *Org. Lett.* **2015**, *17*, 2458–2461; d) H. Wang, H. R. Tong, G. He, G. Chen, *Angew. Chem. Int. Ed.* **2016**, *55*, 15387–15391; e) J. P. Reid, J. M. Goodman, *Chem. Eur. J.* **2017**, *23*, 14248–14260; f) L. Yang, R. Melot, M. Neuburger, O. Baudoin, *Chem. Sci.* **2017**, *8*, 1344–1349; g) R. Maji, S. C. Mallojjala, S. E. Wheeler, *Chem. Soc. Rev.* **2018**, *47*, 1142–1158; h) P.-S. Wang, L.-Z. Gong, *Synthesis* **2022**, *54*, 4795–4801.

[17] Deposition number 2130315 (**3j**) contains the supplementary crystallographic data for this paper. These data are provided free of charge by the joint Cambridge Crystallographic Data Centre and Fachinformationszentrum Karlsruhe Access Structures service.

[18] a) The Gibbs free energies of important stationary points are provided in Table S9 in the Supporting Information. There have been a number of reports on the use of the B3LYP-D3 function for studying transition metal catalyzed reactions; b) Computational details are provided in the computational methods section in the Supporting Information; c) P. A. Provencher, J. F. Hoskin, J. J. Wong, X. Chen, J.-Q. Yu, K. Houk, E. J. Sorensen, *J. Am. Chem. Soc.* **2021**, *143*, 20035–20041; d) B. Bhaskararao, M. E. Rotella, D. Y. Kim, J.-M. Kee, K. S. Kim, M. C. Kozlowski, *J. Am. Chem. Soc.* **2022**, *144*, 16171–16183; e) S. Chatterjee, I. Harden, G. Bistoni, R. G. Castillo, S. Chabbra, M. van Gastel, A. Schnegg, E. Bill, J. A. Birrell, B. Morandi, *J. Am. Chem. Soc.* **2022**, *144*, 2637–2656; f) P.-P. Chen, P. Wipf, K. Houk, *Nat. Commun.* **2022**, *13*, 7292; g) Z. Ren, D. G. Musaev, H. M. Davies, *ACS Catal.* **2022**, *12*, 13446–13456; h) S. Ghosh, A. Changotra, D. A. Petrone, M. Isomura, E. M. Carreira, R. B. Sunoj, *J. Am. Chem. Soc.* **2023**, *145*, 2884–2900.

[19] S. Ghosh, S. Shilpa, C. Athira, R. B. Sunoj, *Top. Catal.* **2022**, *65*, 141–164.

[20] G. Jindal, R. B. Sunoj, *J. Am. Chem. Soc.* **2014**, *136*, 15998–16008.

[21] a) Details of different possibilities considered for the formation of a potential active catalyst from the pre-catalyst is provided in Figure S1 in the Supporting Information; b, It is found that the inclusion of (S_a)-CPA as a counterion results in significant stabilization of the active catalyst. .

[22] See Figure S5 in the Supporting Information for the C–H activation pathway involving different ligands, bases and additives in the CMD mechanism.

[23] The Gibbs free energy profile for (S_a)-CPA assisted and unassisted migratory insertion step is provided in Figure S6 and Table S6 in the Supporting Information.

[24] See Figure S8 in the Supporting Information for the Gibbs free energy profile devoid of (S_a)-CPA. It can be noticed that the *si*-I mode of migratory insertion through **[6c′–7c′]**‡ is 0.5 kcal/mol lower than the *re*-I mode. Such a difference in TS energies corresponds to a diastereoselectivity of 39 %, consistent with the observed low diastereoselectivity under experimental conditions.

[25] a) A similar energetic trend was observed by using a different fluoro-group containing biaryl substrate. The computed Gibbs free energy profile is shown in Figure S8 in the Supporting Information; b) The overall energetic features of the catalytic cycle can be understood using the relative Gibbs free energies of important transition states and intermediates provided in Table S7.

[26] a) The details of single point energy calculations using the M06, ωB97X-D, and B03LYP-D03-BJ functionals are provided in Table S10 in the Supporting Information. The mechanistic trends such as the identity of the turn-over determining step, stereoselectivity predictions, and the overall conclusions obtained using different functionals were found to be very similar; b) The optimized geometries of important transition states are shown in Figure S11 in the Supporting Information.

[27] a) S. Kozuch, S. Shaik, *Acc. Chem. Res.* **2011**, *44*, 101–110; b) S. Kozuch, *Wiley Interdiscip. Rev.: Comput. Mol. Sci.* **2012**, *2*, 795–815.

[28] To obtain maximum δE, different likely combinations of the stationary points involved in the catalytic cycle are considered. The energetic span calculations are shown in Table S7 in the Supporting Information.

[29] The computed kinetic isotope effect (KIE) for the C–H activation step is found to be 1.00, which is in good agreement

with the experimental observations. See Table S11 in the Supporting Information for more details.
[30] E. M. Simmons, J. F. Hartwig, *Angew. Chem. Int. Ed.* **2012**, *51*, 3066–3072.
[31] The rotational barrier for (S_a) to (R_a) interconversion for the low yielding substrates **1c**, **1j**, and **1p** are 22.0, 19.1, and 18.2 kcal/mol respectively, which is energetically favored under reaction conditions. Therefore, the reaction is most likely proceeding via a dynamic kinetic resolution (DKR) pathway.
[32] The Gibbs free energy profile diagram for the migratory insertion step for activated and unactivated olefins is provided in Figure S10 in the Supporting Information.
[33] a) F. M. Bickelhaupt, *J. Comput. Chem.* **1999**, *20*, 114–128; b) F. M. Bickelhaupt, K. N. Houk, *Angew. Chem. Int. Ed.* **2017**, *56*, 10070–10086.
[34] a) The transition state is partitioned into three components, i.e, olefin, (S_a)-CPA and the remaining catalyst-substrate counterpart shown in Figure S8 in the Supporting Information. ; b) Details regarding the activation strain analysis are provided in Table S8 in the Supporting Information.

Manuscript received: July 16, 2023
Accepted manuscript online: November 23, 2023
Version of record online: December 6, 2023